Therefore, if $(dT_c/dP)$ is negative, $(\partial^2\Delta V_M/\partial\phi_2^2)_c$ is positive or $\Delta V_M$ is negative, while a positive $(dT_c/dP)$ corresponds to positive $\Delta V_M$. It is speculated that the value of excess volume of mixing $\Delta V_M$ in PS/DEO changes from negative to positive with increasing pressure over 1–1000 atm for solutions with $M_w > 5.0 \times 10^4$, while in solutions with $M_w = 1.67 \times 10^4$, values of $\Delta V_M$ are positive over 1–50 atm.

Since eq 2 with values of $c_1\nu^2 = 0.0339$ and $c_1\tau^2 = 0.0652$ also predicts the upper and lower critical solution temperatures in PS/DEO, eq 2 is very useful for predicting the phase separation behaviors in polymer solutions over wide temperature and pressure ranges.

## Discussion

In this calculation we have adopted two approximations. The first is neglect of the $\tilde{\beta}_1\tilde{P}_1/\tilde{\alpha}_1\tilde{T}_1$ term in eq 2, which means that a direct contribution of the $\tilde{P}_1\tilde{V}_1$ term to the $\chi_1$ parameter is negligibly small compared to that of the $\tilde{C}_{p,1}\tau^2$ term. The former is related to $(\partial^2\tilde{G}/\partial\tilde{P}_1\tilde{T}_1)$ and $(\partial^2\tilde{G}/\partial\tilde{P}_1^2)$, while the latter is originally related to $(\partial^2\tilde{G}/\partial\tilde{T}_1^2)$. In this work we have obtained that the experimental behavior of the UCST against pressure in PS/DEO can be predicted through the two terms, $(-\tilde{U}_1/\tilde{T}_1)\nu^2$ and $\tilde{C}_{p,1}\tau^2/2$ without the $\tilde{\beta}_1\tilde{P}_1/\tilde{\alpha}_1\tilde{T}_1$ term in eq 2. It is also found from the calculation that the term $\tilde{P}_1\tilde{V}_1^2/(\tilde{P}_1\tilde{V}_1^2 + 1)$ corresponding to $\tilde{\beta}_1\tilde{P}_1/\tilde{\alpha}_1\tilde{T}_1$ in eq 6 is an increasing function of pressure, and therefore the term may cause a poor prediction of the experimental results because the second term in eq 2 changes to an increasing function of pressure from a decreasing one with the introduction of $\tilde{P}_1\tilde{V}_1^2/(\tilde{P}_1\tilde{V}_1^2 + 1)$ term. However, the large difference between the calculated values and experimental ones observed in low molecular weight PS may be improved by introducing the contribution of the $\tilde{\beta}_1\tilde{P}_1/\tilde{\alpha}_1\tilde{T}_1$ term to $\chi_1$. The other approximation is related in that the $\chi_1$ parameter is independent of concentration. Although the approximation is not accepted experimentally, we can obtain useful information on the general aspect of phase separation behavior under pressure for dilute polymer solutions near the critical concentration through eq 9.

It is interesting to refer to theoretical works on the polymer–solvent interaction parameter. A closed expression for $\chi$ as a function of concentration has been derived by Koningsveld and Kleintjens[24] by taking account of the distinction between the site fraction and volume fraction. Sanchez and co-workers[25,26] have applied the lattice-fluid theory to polymer solutions. Whether these theories can explain the pressure dependence of the UCST obtained in this work depends on whether the pressure dependence of the $\chi$ parameter in these theories is expressed by the parabolic-like function of pressure with a minimum.

**Registry No.** PS, 9003-53-6; DEO, 95-92-1.

## References and Notes


(1) Freeman, P. I.; Rowlinson, J. S. *Polymer* **1960**, *1*, 20.
(2) Flory, P. J.; Orwoll, R. A.; Vrij, A. *J. Am. Chem. Soc.* **1964**, *86*, 3507.
(3) Flory, P. J. *J. Am. Chem. Soc.* **1965**, *87*, 1833.
(4) Patterson, D.; Delmas, G. *Trans. Faraday Soc.* **1969**, *61*, 708.
(5) Cowie, J. M. G.; Maconnachie, A.; Ranson, R. J. *Macromolecules* **1971**, *4*, 57.
(6) Siow, K. S.; Delmas, G.; Patterson, D. *Macromolecules* **1972**, *5*, 29.
(7) Saeki, S.; Kuwahara, N.; Konno, S.; Kaneko, M. *Macromolecules* **1973**, *6*, 246.
(8) Davenport, A. J.; Rowlinson, J. S.; Saville, G. *Trans. Faraday Soc.* **1966**, *62*, 322.
(9) Scott, R. L.; van Konynenburg, P. H. *Discuss. Faraday Soc.* **1970**, *49*, 87.
(10) Cowie, J. M. G.; Saeki, S. *Polym. Bull. (Berlin)* **1981**, *6*, 75.
(11) Ehrlich, P.; Kurpen, J. J. *J. Polym. Sci., Part A* **1963**, *1*, 3217.
(12) Schneider, G. M. *Adv. Chem. Phys.* **1970**, *16*, 1.
(13) Zeman, L.; Patterson, D. *J. Phys. Chem.* **1972**, *76*, 1214.
(14) Zeman, L.; Biros, J.; Delmas, G.; Patterson, D. *J. Phys. Chem.* **1972**, *76*, 1206.
(15) Saeki, S.; Kuwahara, N.; Nakata, M.; Kaneko, M. *Polymer* **1975**, *16*, 445.
(16) Saeki, S.; Kuwahara, N.; Kaneko, M. *Macromolecules* **1976**, *9*, 101.
(17) Saeki, S.; Kuwahara, N.; Nakata, M.; Kaneko, M. *Polymer* **1976**, *17*, 685.
(18) Onodera, M. *J. Polym. Sci., Polym. Symp.* **1977**, *No. 61*, 271.
(19) Ishizawa, M.; Kuwahara, N.; Nakata, M.; Nagayama, W.; Kaneko, M. *Macromolecules* **1978**, *11*, 871.
(20) Nakata, M.; Kuwahara, N.; Kaneko, M. *J. Chem. Phys.* **1975**, *62*, 4278.
(21) Flory, P. J. *Principles of Polymer Chemistry*; Cornell University: Ithaca, NY, 1953.
(22) Hocker, H.; Blake, G. J.; Flory, P. J. *Trans. Faraday Soc.* **1971**, *67*, 2251.
(23) Prigogine, I.; Defey, R. *Chemical Thermodynamics*; Longmans: London, 1954.
(24) Koningsveld, R.; Kleintjens, L. A. *Macromolecules* **1971**, *4*, 637.
(25) Lacombe, R. H.; Sanchez, I. C. *J. Phys. Chem.* **1976**, *80*, 2568.
(26) Sanchez, I. C.; Lacombe, R. H. *Macromolecules* **1978**, *11*, 1145.


# Static Structure Factor of Charged Reptating Polymer Chains


**Gary W. Slater* and Jaan Noolandi***

*Xerox Research Centre of Canada, 2660 Speakman Drive, Mississauga, Ontario, Canada L5K 2L1.*

*Received January 17, 1986*


ABSTRACT: Using the biased reptation model that we have introduced recently to understand DNA gel electrophoresis, we study here the static structure factor of highly entangled charged polymer chains in an electric field. The relevant time and length scales are found and interpreted in terms of the dynamics of the chains. The exact structure factor is given for some examples. The possibility of studying such systems by small-angle neutron scattering and computer simulations is discussed.


## 1. Introduction

One of the most popular models for highly entangled polymer systems is the so-called reptation model.[1-3] Conceptually easy to understand, it leads to relatively simple calculations of various rheological parameters.[3] The nonequilibrium correlation function of a reptating chain has also been calculated with this model;[4,5] the time-dependence of the static structure factor of a uniaxially stretched coil has been obtained from these results and compared with available data from small-angle neutron scattering (SANS) experiments.[6]

Recently, we introduced a biased reptation model (BRM) to study the problem of DNA gel electrophoresis.[7] This model predicts that the electric forces together with

0024-9297/86/2219-2356$01.50/0 

the reptation mechanism lead to a stretching of the DNA chain conformations in the field direction.[7-9] It was found that this stretching of the conformations modifies the electrophoretic properties of long DNA chains.[9-10] Calculation of the time constants for the dynamics of the DNA chains based on this model has been successful in explaining pulsed field electrophoresis results.[9]

We show here how, using the BRM (section 2), one can calculate the static structure factor of charged chains in electric fields (section 3). From the relevant parameters, we then identify the time and length scales which dictate the behavior of the system (section 5). The solution of the equations has to be found numerically in general, or a computer simulation must be carried out; in section 6, however, we present some exact results for a simple case. We believe that this study clarifies the mechanism by which chains separate in gel electrophoresis and gives information on the importance of the chain ends in the reptation dynamics.

## 2. Biased Reptation Model

In the BRM, as well as in the usual reptation model, the chain is enclosed (or trapped) in an open-ended tube of contour length $L$ defined by the entanglements surrounding it. The tube renewal takes place only from the ends, and the motion of the chain in the tube is essentially one-dimensional. The Langevin equations for the dynamics of a reptating effective bead–rod chain are given by[3]

$$\mathbf{R}_n(t + \Delta t) = \tfrac{1}{2}[1 + \eta(t)]\mathbf{R}_{n+1}(t) + \tfrac{1}{2}[1 - \eta(t)]\mathbf{R}_{n-1}(t) \tag{1}$$

where $\mathbf{R}_1(t)$, $\mathbf{R}_2(t)$, ..., $\mathbf{R}_{N+1}(t)$ are the positions of the $N + 1$ beads of the chain, and $\eta(t)$ is a stochastic function which takes the value of +1 for a forward jump along the tube axis, and −1 for a backward jump. Here $\Delta t$ is the average time taken by the chain to move the average distance $a$ between entanglements ($a = \langle|\mathbf{R}_{i+1}(t) - \mathbf{R}_i(t)|\rangle = L/N$); the two are related to the curvilinear diffusion constant $D_c$ and the friction coefficient $\xi_c$ by

$$D_c = \frac{k_B T}{\xi_c} = \frac{a^2}{2\Delta t} \tag{2}$$

The vectors $\mathbf{R}_0(t)$ and $\mathbf{R}_{N+2}(t)$ give the possible positions of the ends after a backward or a forward jump, respectively. These boundary conditions are defined by

$$\mathbf{R}_0(t) = \mathbf{R}_1(t) + \mathbf{a}_1(t) \tag{3}$$

$$\mathbf{R}_{N+2}(t) = \mathbf{R}_{N+1}(t) + \mathbf{a}_N(t) \tag{4}$$

where $\mathbf{a}_1(t)$ and $\mathbf{a}_N(t)$ are the vectors creating a new portion of the tube during each jump. In other words,[7] during a forward jump, the $\mathbf{r}_N$ ($\equiv\mathbf{R}_{N+1}(t) - \mathbf{R}_N(t)$) segment leaves the tube and takes the direction $\mathbf{a}_N(t)$; similarly, during a backward jump, the $\mathbf{r}_1$ segment leaves the tube to take the direction $-\mathbf{a}_1(t)$.

In the absence of an electric field, the thermal movement of the chain is perfectly random: the probabilities $p_+(t)$ of having a forward jump at time $t$ ($\eta(t) = +1$) and $p_-(t)$ of having a backward jump ($\eta(t) = -1$), are equal ($p_+(t) = p_-(t) = \frac{1}{2}$), and the tube-generating vectors $\mathbf{a}_{1,N}(t)$ are stochastic vectors of random direction ($\langle\mathbf{a}_{1,N}(t)\rangle = 0$) and constant magnitude $a$.

When an electric field $\mathbf{E} = E\hat{x}$ is applied, the electric forces acting on the charged parts of the chain modify this picture. In general, we can consider that the field biases both the probabilities $p_\pm$ and the directions the vectors $\mathbf{a}_{1,N}(t)$ can take; in the case of a uniformly charged chain, we have shown that this increases the average end-to-end distance in the field direction,[7-9] leading to a field-dependent and molecular-weight-independent electrophoretic mobility,[9] in agreement with available experimental results on DNA.

The vectors $\mathbf{a}_{1,N}(t)$ will orient preferentially in the field direction.[7,9] For an uncharged end segment, the (isotropic) probability $g_0(\theta)\,d\theta$ that a vector $\mathbf{a}(t)$ at time $t$ makes an angle $\theta(t)$ between $\theta$ and $\theta + d\theta$ with the field direction (Figure 1) is simply $g_0(\theta)\,d\theta = \frac{1}{2}\sin\theta\,d\theta$, with $0 \le \theta \le \pi$. For a charged end-segment $\mathbf{r}_{1,N}$ of length $a$ having a uniformly distributed charge $Q_{1,N}$, this distribution function is[9]

$$g_{1,N}(\theta)\,d\theta = (g_0(\theta)\,d\theta)[\theta^*_{1,N}\exp(\theta^*_{1,N}\cos\theta)/\sinh\theta^*_{1,N}] \tag{5}$$

where

$$\theta^*_{1,N} \equiv Q_{1,N}Ea/2k_BT \tag{6}$$

The extra term in brackets is a normalized Boltzmann factor which weights the relative probabilities of the possible orientations of the vectors $\mathbf{a}_{1,N}(t)$ in the field $\mathbf{E}$. Using (5), we can calculate the average angle between $\mathbf{E}$ and the vectors $\mathbf{a}_{1,N}(t)$:

$$\langle\cos\theta\rangle_0 = 0 \tag{7a}$$

$$\langle\cos\theta\rangle_{Q_{1,N}} = \coth(\theta^*_{1,N}) - 1/(\theta^*_{1,N}) \tag{7b}$$

$$\simeq (\theta^*_{1,N})/3 - (\theta^*_{1,N})^3/45 + \ldots \qquad \text{for } \theta^*_{1,N} \ll 1 \tag{7c}$$

$$\langle\cos^2\theta\rangle_0 = \tfrac{1}{3} \tag{8a}$$

$$\langle\cos^2\theta\rangle_{Q_{1,N}} = 1 + \frac{2}{(\theta^*_{1,N})^2} - \frac{2\coth(\theta^*_{1,N})}{\theta^*_{1,N}} \tag{8b}$$

$$\simeq \frac{1}{3}\left(1 + \frac{2(\theta^*_{1,N})^2}{15} + \ldots\right) \qquad \text{for } (\theta^*_{1,N})^2 \ll 1 \tag{8c}$$

In many cases of interest, $\theta^* \le 1$, and (7c) and (8c) are good approximations. The two ends are equivalent only if $Q_1 = Q_N$.

The electric forces also generate a net *instantaneous longitudinal* force $F_l(\mathbf{E},t)$ on a given chain in its tube[11] (lateral movements are hindered by the tube). This force leads, for this chain, to the net instantaneous longitudinal velocity[11]

$$v_l(\mathbf{E},t) = F_l(\mathbf{E},t)/\xi_c \tag{9}$$

In the BRM,[7,9] this velocity is equivalent to an *instantaneous* bias in the probabilities $p_\pm(\mathbf{E},t)$; writing it as

$$p_\pm(\mathbf{E},t) = \tfrac{1}{2}[1 \pm \delta(\mathbf{E},t)] \tag{10}$$

we see that the bias $\delta(\mathbf{E},t)$ and the longitudinal velocity $v_l(\mathbf{E},t)$ are related simply by $v_l = a\delta/\Delta t$. Comparing to (9), we get the following expression for the necessary instantaneous bias:

$$\delta(\mathbf{E},t) = F_l(\mathbf{E},t)a/2k_BT \tag{11}$$

where we have used (2). Therefore, the bias is simply, for a given chain, the ratio between the instantaneous energy of one segment under the tension $F_l(\mathbf{E},t)$ and the thermal energy.[9]

In general, $F_l$ and $\delta$ will be conformation- and field-dependent for a given chain and, hence, time-dependent even in a constant electric field. The simple case where $\delta$ *is only field-dependent* is more mathematically tractable since the value of $\delta(\mathbf{E})$ is then the same for all chain conformations; such an example is treated in section 6.

The BRM holds only for $\delta \leq 1$; at "very" high fields, the stochastic model is invalid as the chain moves along its tube axis at a velocity greater than $a/\Delta t$. Our main interest resides in the study of cases for which the thermal Brownian motion and the electric drift $v_1$ interfere ($\delta \leq 1$).

Finally, note that the BRM does not take into account intra- or interchain interactions[12] (**E** always refers to the external electric field); its limitations are discussed in section 8.

It should be noted here that the model of Lumpkin et al.[10] is equivalent to having $\delta \geq 1$ and $Q_1 = Q_N$ in the BRM and can only be used to study the steady-state properties of DNA-like chains. Our model is much more general but is limited to $\delta \leq 1$.

## 3. Static Structure Factor

The correlation function $G_{mn}(\mathbf{R},t)$ is defined as the probability that the $m$th and the $n$th segments of the chain are separated by a distance **R** at time $t$:

$$G_{mn}(\mathbf{R},t) = \langle \delta\{[\mathbf{R}_m(t) - \mathbf{R}_n(t)] - \mathbf{R}\}\rangle \tag{12}$$

The structure factor $S(\mathbf{q},t)$ measured in elastic neutron scattering is defined in terms of the Fourier transform of $G_{mn}(\mathbf{R},t)$:

$$S(\mathbf{q},t) = \frac{1}{N^2}\sum_{mn} F_{mn}(\mathbf{q},t) \tag{13}$$

$$F_{mn}(\mathbf{q},t) = \int \mathrm{d}^3R\, e^{i\mathbf{q}\cdot\mathbf{r}} G_{mn}(\mathbf{R},t) = \langle \exp\{i\mathbf{q}\cdot[\mathbf{R}_m(t) - \mathbf{R}_n(t)]\}\rangle \tag{14}$$

where the averages $\langle ... \rangle$ are carried out for a nonequilibrium ensemble of identical chains. Since the reptation model does not deal with intramolecular degrees of freedom, the case of interest here is clearly $qa \ll 1$.

**3.1. General Case.** The static structure factor $S(\mathbf{q},t)$ can be computed from the definitions (13) and (14), the Langevin equation (1), the boundary conditions (3) and (4), and the biases given by (7), (8), (10), and (11).

Since the boundary conditions (3) and (4) do not depend upon $p_\pm(\mathbf{E},t)$ for each chain, the boundary conditions for $F_{mn}(\mathbf{q},t)$ are always time-independent in a constant electric field; moreover, they are the same for all the chains of a given mixture, which will be of great importance for the discussion of section 5. Using (14), one can write from (3) and (4)

$$F_{m0}(\mathbf{q},t) = F_{m1}(\mathbf{q},t)\langle \exp[-i\mathbf{q}\cdot\mathbf{a}_1(t)]\rangle \tag{15a}$$

$$F_{0n}(\mathbf{q},t) = F_{1n}(\mathbf{q},t)\langle \exp[+i\mathbf{q}\cdot\mathbf{a}_1(t)]\rangle \tag{15b}$$

$$F_{N+2\,n}(\mathbf{q},t) = F_{N+1\,n}(\mathbf{q},t)\langle \exp[+i\mathbf{q}\cdot\mathbf{a}_N(t)]\rangle \tag{15c}$$

$$F_{m\,N+2}(\mathbf{q},t) = F_{m\,N+1}(\mathbf{q},t)\langle \exp[-i\mathbf{q}\cdot\mathbf{a}_N(t)]\rangle \tag{15d}$$

Using (5), we obtain, for $qa \ll 1$,

$$\langle \exp[\pm i\mathbf{q}\cdot\mathbf{a}_j(t)]\rangle = 1 \pm i\langle \mathbf{q}\cdot\mathbf{a}_j(t)\rangle - \langle [\mathbf{q}\cdot\mathbf{a}_j(t)]^2\rangle/2 + ... = 1 \pm i\frac{az_j}{L} - \frac{ax_j}{L} + ... \tag{16}$$

with

$$z_j \equiv L\langle \mathbf{q}\cdot\mathbf{a}_j(t)\rangle/a = Lq\cos\psi\langle\cos\theta\rangle_{Q_j} \tag{17a}$$

$$x_j = \frac{L}{2a}\langle [\mathbf{q}\cdot\mathbf{a}_j(t)]^2\rangle = \tfrac{1}{2}q^2La[\tfrac{1}{2}\sin^2\psi + (\cos^2\psi - \tfrac{1}{2}\sin^2\psi)\langle\cos^2\theta\rangle_{Q_j}] \tag{17b}$$

where $\psi$ is the angle between **q** and **E** (Figure 1) and $\langle \cos\theta\rangle_{Q_j}$ and $\langle\cos^2\theta\rangle_{Q_j}$ are given by (7) and (8) with the corresponding $\theta^*_j$ for the given ($j$th) end of the chain ($j = 1, N$).

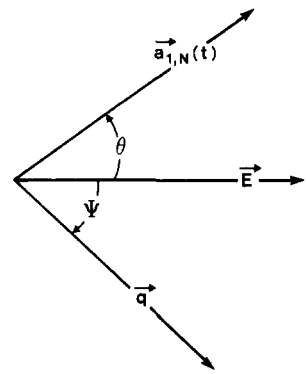


**Figure 1.** The random vectors $\mathbf{a}_{1,N}(t)$ make an angle $\theta$ with the direction of the electric field **E**, while the **q** vector makes an angle $\psi$ with **E**. Note that the three vectors are not coplanar in general.

Defining $l = ma$ and $l' = na$, we obtain the following continuum limit of (15) for large $N$:

$$\frac{\partial F(l,l',\mathbf{q},t)}{\partial l'} = \frac{iz_1 + x_1}{L}F(l,l',\mathbf{q},t) \qquad \text{at } l' = 0 \tag{18a}$$

$$\frac{\partial F(l,l',\mathbf{q},t)}{\partial l} = \frac{-iz_1 + x_1}{L}F(l,l',\mathbf{q},t) \qquad \text{at } l = 0 \tag{18b}$$

$$\frac{\partial F(l,l',\mathbf{q},t)}{\partial l} = \frac{iz_N - x_N}{L}F(l,l',\mathbf{q},t) \qquad \text{at } l = L \tag{18c}$$

$$\frac{\partial F(l,l',\mathbf{q},t)}{\partial l'} = \frac{-iz_N - x_N}{L}F(l,l',\mathbf{q},t) \qquad \text{at } l' = L \tag{18d}$$

where $F(l,l',\mathbf{q},t) \equiv F_{mn}(\mathbf{q},t)$.

In the general case of a conformation- and time-dependent bias $\delta(\mathbf{E},t)$, an exact equation cannot be found for $F_{mn}(\mathbf{q},t)$ or $F(l,l',\mathbf{q},t)$ from the Langevin equation (1). A computer simulation is then the simplest way to obtain the static structure factor.

**3.2. Time-Independent Bias.** In order to obtain some analytic results, we assume that $\delta$ is a conformation- (and time-) independent parameter or else that a suitable average value $\langle\delta(\mathbf{E})\rangle$ can be found.

From equations (1), (10), and (14), $F_{mn}(\mathbf{q},t)$ then satisfies

$$F_{mn}(\mathbf{q},t + \Delta t) = \tfrac{1}{2}[1 + \delta(\mathbf{E})]F_{m+1\,n+1}(\mathbf{q},t) + \tfrac{1}{2}[1 - \delta(\mathbf{E})]F_{m-1\,n-1}(\mathbf{q},t) \tag{19}$$

This equation is invalid if the bias $\delta$ is conformation-dependent, as is the case for a uniformly charged chain.[7,8]

With $l = ma$ and $l' = na$, the continuum limit of (19) for large $N$ and small $\delta$ gives the following differential equation:

$$\frac{\partial F(l,l',\mathbf{q},t)}{\partial t} = D_c\left(\frac{\partial}{\partial l} + \frac{\partial}{\partial l'}\right)^2 F(l,l',\mathbf{q},t) + \frac{2D_c}{a}\delta(\mathbf{E})\left(\frac{\partial}{\partial l} + \frac{\partial}{\partial l'}\right)F(l,l',\mathbf{q},t) \tag{20}$$

with the boundary conditions given by eq (18). It should be noted that this continuum limit can be used only to study cases were the relevant chain conformations are not expected to contain sharp structures, i.e., structures with a length scale of order $\sim a$.

To solve (18) and (20), we use the variables

$$s = (l + l')/L; \qquad p = (l - l')/L \tag{21}$$

Equations 18 and 20 then become

$$\left(\frac{\partial}{\partial s} - \frac{\partial}{\partial p}\right)F(s,p,\mathbf{q},t) = (iz_1 + x_1)F(s,p,\mathbf{q},t) \qquad \text{at } s = p \tag{22a}$$

$$\left(\frac{\partial}{\partial s} + \frac{\partial}{\partial p}\right)F(s,p,\mathbf{q},t) = (-iz_1 + x_1)F(s,p,\mathbf{q},t) \quad \text{at } s = -p \qquad (22b)$$

$$\left(\frac{\partial}{\partial s} + \frac{\partial}{\partial p}\right)F(s,p,\mathbf{q},t) = (iz_N - x_N)F(s,p,\mathbf{q},t) \quad \text{at } s = 2 - p \qquad (22c)$$

$$\left(\frac{\partial}{\partial s} - \frac{\partial}{\partial p}\right)F(s,p,\mathbf{q},t) = (-iz_N - x_N)F(s,p,\mathbf{q},t) \quad \text{at } s = 2 + p \qquad (22d)$$

$$\frac{\partial F(s,p,\mathbf{q},t)}{\partial t} = \frac{4D_c}{L^2}\frac{\partial^2 F(s,p,\mathbf{q},t)}{\partial s^2} + \frac{4D_c}{La}\delta(\mathbf{E})\frac{\partial F(s,p,\mathbf{q},t)}{\partial s} \qquad (23)$$

The problem is therefore reduced to solving (22)–(23) with the values of $x_{1,N}$ and $z_{1,N}$ appropriate for the charges on the end segments $\mathbf{r}_1$ and $\mathbf{r}_N$. The boundary conditions (22a) and (22c) are for $p > 0$ (i.e., $l > l'$), while (22b) and (22d) are for $p < 0$ (i.e., $l < l'$).

Finally, in terms of the relative variables $s$ and $p$, the structure factor $\mathbf{S}(\mathbf{q},t)$ is given by

$$S(\mathbf{q},t) = \tfrac{1}{2}\int_0^1 ds \int_{-s}^{s} dp\, F(s,p,\mathbf{q},t) + \tfrac{1}{2}\int_1^2 ds \int_{s-2}^{2-s} dp\, F(s,p,\mathbf{q},t) \qquad (24)$$

In the steady state, i.e., for $t \to \infty$, we have $\partial F/\partial t = 0$, and the general solution of (23) has the form

$$F_\infty(s,p,\mathbf{q}) = A(p)\left[\frac{1 - e^{-\Delta s}}{\Delta}\right] + C(p) \qquad (25)$$

where $\Delta = \Delta(\mathbf{E}) = N\delta(\mathbf{E})$. The "constants" of integration $A(p)$ and $C(p)$ are to be found by the boundary conditions (22). The steady state evolves from any initial condition after the field has been applied for an infinitely long time.

Of particular interest is the time scale of relaxation of an initial condition $F_0(s,p,\mathbf{q},t = 0)$ toward the steady-state $F_\infty(s,p,\mathbf{q},t = \infty)$. In the time-dependent case, the solution of (23) is found in terms of the Laplace transform:[5]

$$F^*(s,p,\mathbf{q},\omega) = \int_0^\infty dt\, e^{-\omega t}F(s,p,\mathbf{q},t) \qquad (26)$$

Equation 23 then becomes

$$\omega F^*(s,p,\mathbf{q},\omega) - F_0 = \frac{4D_c}{L^2}\frac{\partial^2 F^*(s,p,\mathbf{q},\omega)}{\partial s^2} + \frac{4D_c}{L^2}\Delta(\mathbf{E})\frac{\partial F^*(s,p,\mathbf{q},\omega)}{\partial s} \qquad (27)$$

For an initial condition of the form $F_0(s,p,\mathbf{q},t = 0) = e^{-\beta p}$, which includes the case of a chain at equilibrium at $t = 0$ (see (33)), the general solution to eq 27 is

$$F^*(s,p,\mathbf{q},w) = \frac{1}{w}\{F_0(s,p,\mathbf{q},t = 0) + A_+(p)e^{u_+ s} + A_-(p)e^{u_- s}\} \qquad (28)$$

where the "constants" of integration $A_\pm(p)$ are also to be determined by the boundary conditions (22), and

$$u_\pm = -\tfrac{1}{2}\Delta \pm [u_0^2 + \tfrac{1}{4}\Delta^2]^{1/2} \qquad (29)$$

$$u_0 = \left[\frac{wL^2}{4D_c}\right]^{1/2} \qquad (30)$$

For $\delta = 0$, eq 29 gives $u_\pm = \pm u_0$, and we find the solution given in ref 5. For $\delta \neq 0$, we have two important limits.

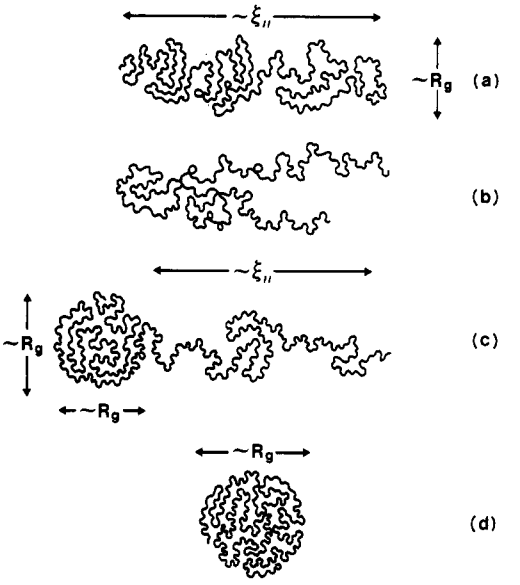


**Figure 2.** Typical high-field conformations for the four classes of charged polymer chains. (a) $Q_1Q_N < 0$: the end segments point in opposite directions, and the chain stretches to take an I shape. (b) $Q_1Q_N > 0$: the end segments point in the same direction, giving a J shape conformation. (c) Only one end segment is charged: this segment stretches a part of the chain, while the rest stays in a zero-field-like random-walk conformation. (d) $Q_1 = Q_N = 0$: we have a random-walk conformation even if the rest of the chain is charged (i.e., even if $\langle\delta(\mathbf{E})\rangle \neq 0$).

At $\omega \to 0$, which corresponds to $t \to \infty$, (29) gives $u_+ = 0$ and $u_+ = -\Delta(\mathbf{E})$, in agreement with (25). On the other hand, $\omega \to \infty$ (or $t \to 0$) gives $u_\pm = \pm u_0$; since $A_+(p,\omega \to \infty)e^{+\infty s}$ is unphysical unless $A_+(p,\omega \to \infty) = 0$, (28) reduces to $F = F_0$, as it should be.

We note that the drift (or field-dependent) term becomes the leading term in the differential equations when $\Delta(\mathbf{E}) = N\delta(\mathbf{E}) > 1$ (see eq 27 and 23). This will be interpreted in terms of time scales in section 5.2.

## 4. Zero-Field Case

As an example, we derive here the static structure factor for the equilibrium (zero-field, time-independent) case. According to (7a), (8a), and (17), we have, for $\mathbf{E} = 0$

$$z_1 = z_N = 0 \qquad (31)$$

$$x_1 = x_N \equiv x^{(0)} = q^2\frac{La}{6} = q^2R_g^2 \qquad (32)$$

where $R_g = (La/6)^{1/2}$ is the *radius of gyration of the chain in equilibrium*. The solution of 22–23 is then (with $\delta(E = 0) = \partial F/\partial t = 0$)

$$F_{equ}(s,p,\mathbf{q}) = e^{-q^2R_g^2|p|} \qquad (33)$$

from which (24) gives

$$S_{equ}(\mathbf{q}) = D(q^2R_g^2) \qquad (34a)$$

$$\simeq 1 - \tfrac{1}{3}q^2R_g^2 + \ldots \quad \text{for } qR_g \ll 1 \qquad (34b)$$

$$\simeq 2/q^2R_g^2 \quad \text{for } qR_g \gg 1 \qquad (34c)$$

where $D(x) = 2(x - 1 + e^{-x})/x^2$ is the Debye function. These well-known results indicate that $S_{equ}(\mathbf{q})$ is a measure of the average dimensions of the equilibrium chain.

## 5. Time and Length Scales Involved

The structure factor $S(\mathbf{q},t)$ depends both on the bias $\delta(\mathbf{E},t)$ and on the factors $x_{1,N}$ and $z_{1,N}$. Without knowing the actual function $S(\mathbf{q},t)$, we can draw general conclusions from these parameters. In fact, the length scales involved

in the problem come mainly from $x_{1,N}$ and $z_{1,N}$, while the time scales are easily derived from the diffusion and drift parameters $D_c$ and $\delta(\mathbf{E},t)$ and thus do not depend on the details of the function $S(\mathbf{q},t)$.

In the BRM, there are four different classes of charged chains,[13] defined according to their boundary conditions $x_{1,N}$ and $z_{1,N}$, i.e., according to their end-segment charges $Q_{1,N}$. Figure 2 shows typical examples for each of the four classes. In class a, we have $Q_1Q_N < 0$, and the end segments point in opposite directions in an electric field, thus stretching the chain in an I-shaped conformation, much like an applied external tensile stress. In class b, $Q_1Q_N > 0$, and the end segments are pointing in the same direction, giving a typical J-shaped conformation. In class c, one charge is zero while the other is finite; the electric field then affects only the part of the chain for which the tube has been generated by the charged end segment, the rest of the chain staying in a random-walk conformation (Figure 2c). Finally, when $Q_1 = Q_N = 0$ (Figure 2d), the electric field does not modify the evolution of the tube and, although $\delta$ may well be finite due to charges on other segments, the chain does not depart from its random-walk conformation.

To simplify the discussion that follows, we will assume that for classes a and b above, we have $|Q_1| = |Q_N| = Q$, and we will drop indices 1,$N$ where possible.

**5.1. Length Scales.** There are five obvious length scales in the problem (a sixth one will be introduced in section 6). The first one is $a$, the average distance between entanglements. Usually, we take $a$ as a constant fixed by the topology of the problem; in a gel matrix, $a$ would be given by the average pore size. The scattering techniques usually measure structures at a length scale $q^{-1}$; the reptation theory is valid only for $qa < 1$. A third length is $L = Na$, the length of the tube, which is proportional to the length of the molecule itself.[3]

The last two length scales are related to the boundary conditions $x_{1,N}$ and $z_{1,N}$. The equilibrium conformation ($QE = 0$) is characterized by $R_g$; the ratio between $R_g$ and $q^{-1}$ defines the scattering factor $x_j$. The electric force $Q\mathbf{E}$ brings in the anisotropic conformation length $\xi_\psi$ defined as[13]

$$\xi_\psi = L\langle\cos\theta\rangle|\cos\psi| \tag{35}$$

This length measures the stretching (at an angle $\psi$ from $\mathbf{E}$) of a tube generated by an end segment having an average projection $\langle\cos\theta\rangle$ on the field direction. The ratio between $\xi_\psi$ and $q^{-1}$ defines the boundary condition, $z_j$. Of course, $\xi_\perp = 0$ since the field does not induce order in the transverse plane.

The boundary conditions show a competition between $R_g$ and $\xi_\psi$ if at least one end segment is charged (since $z_j/x_j \sim \xi_\psi/R_g^2$). At low fields, $R_g > \xi_\psi$, and $x_j$ leads to an almost isotropic random-walk conformation (the dependence of $x_j$ upon $\langle\cos^2\theta\rangle$ makes it slightly anisotropic). At large fields, however, we have $R_g > \xi_\perp$ and $R_g < \xi_\parallel$, and $z_{j\parallel}$ leads to a chain conformation that is stretched in the field direction (over a length $\sim\xi_\parallel$), while $x_{j\perp}$ makes it only slightly shrunk in the transverse plane.

For class a chains, strong electric forces lead to I-shaped conformations (Figure 2a), with the average end-to-end distance of order $\xi_\parallel$. For class b, which includes the important case of uniformly charged molecules such as DNA, the chain folds in two (Figure 2b), with both ends pointing in the field direction; the lengths of the two arms of the J-shaped conformation are then proportional to the length $\xi_\parallel$ (at high fields), and the end-to-end distance, i.e., the difference in length between the two arms, depends on the bias factor $\delta$ as well.

In class c, a part (which is a function of the bias $\delta$) of the chain is stretched in the field direction, with an anisotropic characteristic length scale $\xi_\parallel$, while the rest stays in a quasi-isotropic random-walk conformation with the length scale $R_g$ (Figure 2c). Finally, $R_g$ is the only length involved for class d even in high electric fields.

We will see in section 6 that these results can also be reached by finding the appropriate $A(p)$ and $C(p)$ in (25).

**5.2. Time Scales.** Three time scales are important in the reptation theory. The first one is simply $\Delta t$, the microscopic time it takes for a chain to jump over a distance $a$. For $a$ fixed, $\Delta t \sim D_c^{-1} \sim L$.

The de Gennes time $\tau_D$ is the time it takes for the chain to renew completely its tube under the influence of the zero-field Brownian motion. It is defined as[1]

$$\tau_D = \frac{L^2}{\pi^2 D_c} \sim L^3 \tag{36}$$

and also gives the time constant for the relaxation of constraints in field-free reptation.[4-5]

Finally, the longitudinal velocity $v_\parallel(\mathbf{E},t)$ drives its own tube renewal in a time $\tau_E$ defined implicitly by

$$L = \left\langle \left[ \int_0^{\tau_E} v_\parallel(\mathbf{E},t)\, dt \right] \right\rangle_{\text{all chains}} = \left\langle \left[ \frac{2D_c}{a} \int_0^{\tau_E} \delta(\mathbf{E},t)\, dt \right] \right\rangle_{\text{all chains}} \tag{37}$$

(we neglect possible sign reversals of $v_\parallel(\mathbf{E},t)$ here).

The steady state is reached after the initial tube has relaxed to a new one; without an electric field, this occurs in an average time $\tau_D$, while with an electric field alone, this takes an average time $\tau_E$. The true tube disengagement time is due to the combined effect of the thermal motion and of the electric drift. For small fields, $\tau_E \gg \tau_D$, and the zero-field Brownian motion is more effective than the small longitudinal drift $v_\parallel$ in disengaging the chain from its initial tube. For high fields, $\tau_E \ll \tau_D$, and the drift $v_\parallel$ leads to rapid tube disengagement. In these extreme cases, the relaxation of the initial tube conformation therefore takes a time $\tau_{dis} = \min(\tau_D,\tau_E)$.

When $\delta = \delta(\mathbf{E})$, these conclusions are easily obtained analytically; (37) then gives

$$\tau_E(\delta = \delta(\mathbf{E})) \equiv \tau_\delta = \frac{L}{v_\parallel(\mathbf{E})} = \frac{L}{\delta(\mathbf{E})a/\Delta t} = \frac{L^2}{2\Delta(\mathbf{E})D_c} \tag{38}$$

which is also valid for $\delta > 1$. In terms of $\tau_D$ and $\tau_\delta$ (29) becomes

$$u_\pm = \frac{\pi^2}{4}\frac{\tau_D}{\tau_\delta}\left[ -1 \pm \left( 1 + \frac{4\omega\tau_\delta^2}{\pi^2\tau_D} \right)^{1/2} \right] \tag{39}$$

where the competition between the random walk ($\tau_D$) and the electric drift ($\tau_\delta$) is apparent; eq 39 includes both effects for $\delta = \delta(\mathbf{E})$.

When $\tau_\delta \ll \tau_D$ and $\omega\tau_\delta \ll 1$, (39) gives simply $u_+ = 0$ and $u_- = -\Delta(\mathbf{E})$, which agrees with (25) and shows no $\omega$-dependence; consequently, $\tau_\delta$ is then the relevant relaxation time. When $\tau_E \gg \tau_D$ and $\omega\tau_D \ll 1$, one has instead $u_\pm = 0$, which is also $\omega$-independent and agrees with (25) since $\Delta(\mathbf{E}) \simeq \tau_D/\tau_\delta \simeq 0$: $\tau_D$ is the relevant relaxation time here. Therefore, in these extreme cases, the steady-state $F_\infty$ is indeed reached after a time $\tau_{dis} = \min(\tau_D,\tau_\delta)$: at small fields ($\tau_\delta \gg \tau_D$) the Brownian motion is the more effective mechanism, while at large fields ($\tau_\delta \ll \tau_D$), the chain is simply pulled out of its tube by the electric forces.

Using (36) and (38), we find that the large-field limit (for $\delta = \delta(\mathbf{E})$) is at ($\tau_\delta \ll \tau_D$)

$$\delta(\mathbf{E}) = \frac{\Delta(\mathbf{E})}{N} \gg \frac{\pi^2}{2N} \tag{40}$$

which, for a long chain, can be quite small. Therefore, the BRM, valid only for $\delta < 1$, can be used to study this transition from the Brownian regime to the electric drift regime. As noted in section 3, the high-field limit is found approximately at $\Delta(\mathbf{E}) > 1$, i.e., when the drift term in the differential equation (27) is larger than the diffusion term.

## 6. Example 1: Charges of Opposite Signs on the Ends

When the ends of the chain have charges of opposite signs (Figure 2a), we expect a net stretching as the electric forces orient the ends in opposite directions. For simplicity, we assume here that $Q_1 = -Q_N$; we then have, from (6)–(8) and (17),

$$\theta^*_N = -\theta^*_1 \equiv \Theta^* \geq 0; \qquad x_N = x_1 \equiv X \geq 0; \qquad z_N = -z_1 \equiv Z \geq 0 \tag{41}$$

As stated before, we restrict ourselves to cases where the bias $\delta(\mathbf{E})$ is only field-dependent (no dependence upon the conformation of the chains).

In the biased reptation model, the end segments $\mathbf{r}_1$ and $\mathbf{r}_N$ align all the other segments of the chain in the field direction. When (41) is satisfied, it is possible to prove (Appendix A) that the average steady-state (i.e., $t \to \infty$) radius of gyration $G$ is given by

$$G_y^2 = G_z^2 \equiv G_\perp^2 = \frac{Na^2}{12}\langle \sin^2\theta \rangle \tag{42}$$

$$G_x^2 \equiv G_\parallel^2 = \frac{Na^2}{6}\langle \cos^2\theta \rangle + \frac{N^2a^2}{12}\langle \cos\theta \rangle^2 \tag{43}$$

Equations 42 and 43 give $G^2_{x,y,z}(E = 0) = {}^1/_3 R_g^2 = La/18$, as expected. In the low-field regime ($\Theta^* \ll 1$), the radius of gyration is only slightly changed: one has $G_\parallel \geq {}^1/_3 R_g \geq G_\perp$, which means that the average chain stretches slightly in the field direction and reduces its transverse dimension. At very high fields, we have $G_\perp \simeq 0$ and $G_\parallel \simeq L/12^{1/2}$, the radius of gyration of a rod of length $L$, and negligible transverse dimension, as expected. At intermediate fields, we find $G_\perp^2 \simeq R_g^2\langle \sin^2\theta \rangle$ and $G_\parallel \simeq \xi_\parallel$, in agreement with section 5.1.

The steady-state static structure factor contains the details of the response of a stretched chain to neutron scattering. The nonequilibrium (time-dependent) static structure factor indicates how an initial conformation evolves toward a stretched conformation in an electric field.

**6.1. Steady-State Case.** With the scattering factors $X$ and $Z$ defined in (41), the solution to eq 22a and 22c for $A(p)$ and $C(p)$ in (25) are

$$A(p) = K_1 e^{-(X-iZ)} \sinh \Delta(1-p) \tag{44}$$

$$C(p) = e^{-(X-iZ)}\left[-K_1 p e^{-\Delta} - \frac{K_1}{\Delta}\sinh \Delta(1-p) + K_2\right] \tag{45}$$

where the constants $K_{1,2}$ are fixed by the conditions

$$\lim_{p\to 0} F_\infty(s,p,\mathbf{q}) = 1 \tag{46a}$$

$$\lim_{\Delta\to 0}\lim_{Z\to 0}\lim_{X\to x^{(0)}} F_\infty(s,p,\mathbf{q}) = F_{equ}(s,p,\mathbf{q}) \tag{46b}$$

$x^{(0)}$ and $F_{equ}(s,p,\mathbf{q})$ have been defined in section 4. Here we find $K_1 = 0$ and $K_2 = 1$, from which (25), (44), and (45) give

$$F_\infty(s,p > 0,\mathbf{q}) = e^{-(X-iZ)p} \tag{47}$$

This solution reduces to (33) for $E = 0$. Solving (22b), (22d), (46a), and (46b) for $p < 0$, one finds instead $F_\infty(s,p < 0,\mathbf{q}) = e^{+(X+iZ)p}$, from which it is clear that the real part of $F_\infty(s,p,\mathbf{q})$ is even in $p$ while its imaginary part is odd. In this case, (24) gives

$$S_\infty(\mathbf{q}) = 2\,\mathrm{Re}\left\{\int_0^1 ds \int_0^s dp\, F_\infty(s,p > 0,\mathbf{q})\right\} = \mathrm{Re}\, D(X - iZ) = \frac{2X}{X^2+Z^2} + \frac{2(Z^2-X^2)}{(X^2+Z^2)^2} - \frac{2e^{-X}[(Z^2-X^2)\cos Z + 2XZ \sin Z]}{(X^2+Z^2)^2} \tag{48}$$

An interesting aspect of this solution is that it does not include the bias $\delta(\mathbf{E})$, in agreement with Appendix A.

In order to study the different regimes present in the solution (48), we will make use of the fact that $Z = q\xi_\psi$ and $X \sim (qR_g)^2$; i.e., we will study the different wavelength regimes in terms of the length scales $R_g$ and $\xi_\psi$.

**6.1.1. Transverse Structure Factor.** For $\psi = 90°$, the conformation length $\xi_\perp$ is always zero, and one has $Z_\perp = 0$; in this case, the solution (48) reduces to

$$S_\infty^\perp(q) = D(X_\perp) \tag{49a}$$

$$\simeq 1 - {}^1/_3 X_\perp + \ldots \quad \text{for } qR_g < 1 \quad \text{(regime I)} \tag{49b}$$

$$\simeq 2/X_\perp + \ldots \quad \text{for } qR_g > 1 \quad \text{(regime II)} \tag{49c}$$

By comparing eq 34 and 49, we see that the radius of gyration $G_\perp$ is indeed given by (42) in regimes I and II. As expected, the chain transverse dimension collapses ($G_\perp \to 0$; $S^\perp \to 1$) at very high fields.

**6.1.2. Parallel Structure Factor.** More interesting is the $\psi = 0°$ ($\mathbf{q}\parallel\mathbf{E}$) case because one can then have fields high enough for the parallel conformation length $\xi_\parallel$ to be larger than the equilibrium radius of gyration $R_g$.

At *low fields*, i.e., when $\xi_\parallel \ll R_g$, the chain is almost unperturbed by the field. From (48), we then obtain

$$S_\infty^\parallel(q) \simeq 1 - {}^1/_3 X_\parallel + \ldots \quad \text{for } q\xi_\parallel \ll qR_g < 1 \quad \text{(regime III)} \tag{50a}$$

$$S_\infty^\parallel(q) \simeq 2/X_\parallel + \ldots \quad \text{for } \xi_\parallel \ll R_g \text{ and } qR_g > 1 \quad \text{(regime IV)} \tag{50b}$$

By comparing (34), (50), and (43), we see that $S_\infty^\parallel(q)$ also gives a measure of the radius of gyration $G_\parallel$ in regimes III and IV.

At fields large enough to have $\xi_\parallel \gg R_g$, one has to distinguish between four different wavelength regimes; from (48), they are characterized by the following:

$$S_\infty^\parallel(q) \simeq 1 - Z_\parallel^2/12 + \ldots \quad \text{for } 1 > q\xi_\parallel \gg qR_g \quad \text{(regime V)} \tag{51a}$$

$$S_\infty^\parallel(q) \simeq \frac{2(1-\cos Z_\parallel)}{Z_\parallel^2} + \ldots \quad \text{for } qR_g < 1 < q\xi_\parallel \quad \text{(regime VI)} \tag{51b}$$

$$S_\infty^\parallel(q) \simeq 2X_\parallel/Z_\parallel^2 + \ldots \quad \text{for } 1 < q^2R_g^2 < q\xi_\parallel \quad \text{(regime VII)} \tag{51c}$$

$$S_\infty^\parallel(q) = 2/X_\parallel \quad \text{for } 1 < q\xi_\parallel < q^2R_g^2 \quad \text{(regime VIII)} \tag{51d}$$

Regime V is typical of a rod of length $\xi_\parallel$ parallel to $\mathbf{q}$, the radius of gyration $G_\parallel$ of the equivalent rod being given by (43). At intermediate wavelengths (regime VI), we begin to investigate the rodlike chain conformation, but without going to length scales smaller than the equilibrium radius

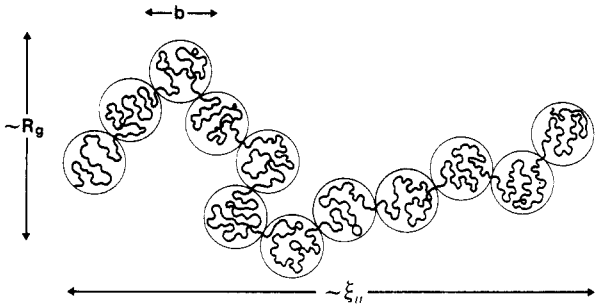


**Figure 3.** Length scales defining the different regimes at high fields. Inside the blobs of size $b \geq a$, the segments are in a random-walk conformation. These blobs are aligned by the field to form a string of length $\xi_\parallel$ and width $R_g$, with $L \geq \xi_\parallel > R_g > b \geq a$.

of gyration $R_g$. Equation 51b then predicts a series of oscillations with a period (in $q$) given by $q_\xi = 2\pi/\xi_\parallel$. The crossover between regimes V and VI takes place at $q = q_\xi/2\pi$.

In regime VII, (51c) predicts an $S_\infty^\parallel(q)$ with very small dependence on $q$. The crossover between regimes VI and VII is at $q = q_g = 1/R_g$. Finally, (51d) shows clearly that the long-range deformation of the chain does not influence the static structure factor at wavenumbers $q > q_b \equiv 1/b = \xi_\parallel/R_g^2$, since $R_g$ is still the only relevant length scale in this limit.

Of course, the oscillations of regime VI will not appear in the spectrum unless we have $q_\xi < q_g$ (otherwise not even one oscillation would occur in the short interval in which this regime is located), i.e., $\xi_\parallel > 2\pi R_g$, which is the case here. Similarly, we require $q_g \ll q_b$ for regime VII, which is equivalent to $\xi_\parallel \gg R_g$. In other words, regimes V–VIII must all show up in the spectrum if we have $\xi_\parallel \gg R_g$.

The *sixth length scale* (see section 5.1) defined by $b = 1/q_b = R_g^2/\xi_\parallel$ can be interpreted in the following way. We see from (51d) that for $q > 1/b$, the static structure factor is the same as for an unstretched chain; i.e., $R_g$ remains the only relevant length scale. This means that the electric forces are not strong enough to modify the random-walk conformations over lengths smaller than $b$. A volume of size $b^3$ contains $n_b \simeq b^2/a^2$ segments if these segments stay in a random-walk conformation; we can therefore see a stretched conformation as a series of $N/n_b$ random-walk "blobs" of size $b$ aligned by the electric forces (which act effectively over lengths larger than $b$). The dimension of the stretched conformation is therefore $(N/n_b)b \simeq \xi_\parallel$, as expected. Since the field does not align the blobs in the transverse direction, they act as effective segments of length $b$ following a transverse random walk with dimension $(N/n_b)^{1/2}b \simeq R_g$. Figure 3 represents a typical stretched conformation showing the breakdown of the chain into blobs of size $b$.

The high-field limit characterized by the alignment of these blobs makes sense only if $b < R_g$, $n_b < N$, and $N/n_b > 1$; these conditions are all equivalent to $\xi_\parallel \gg R_g$.

The description of regimes V–VIII in terms of $b$ and $\xi_\parallel$ is as follows (Figure 3). For $q > 1/b$ (regime VIII) the electric forces are not strong enough to modify the random-walk nature of the conformation, and the structure factor is that for zero field. In the opposite limit where $q < 1/\xi_\parallel$ (regime V), the blobs are aligned to form a quasi-rod of length $\xi_\parallel$, and the structure factor shows the expected radius of gyration $\xi_\parallel/12^{1/2}$. For $1/R_g > q > 1/\xi_\parallel$ (regime VI), we are using a length scale smaller than $\xi_\parallel$ (without being too small to see the blobs); the structure factor shows oscillations with a periodicity $\xi_\parallel$, characteristic again of a rod of length $\xi_\parallel$. Finally, for $1/b > q > 1/R_g$ (regime VII), we probe the blob structure of the rod, and the structure factor reduces to $S_\infty^\parallel(q) \simeq n_b/N$; i.e., the structure factor is then independent of $q$ and gives *a direct measure of the number of blobs.*

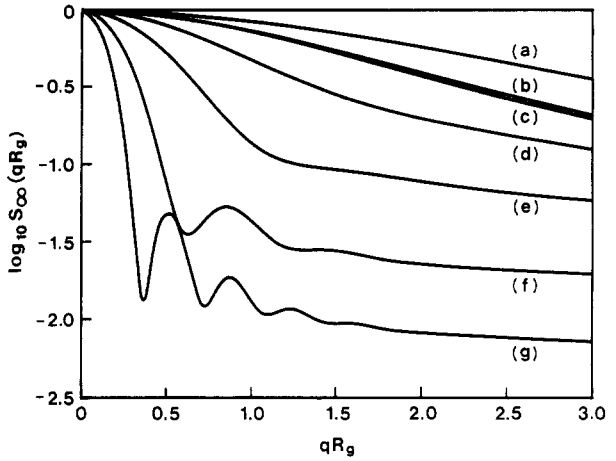


**Figure 4.** Long-wavelength behavior of the steady-state structure factors $S_\infty^\perp$ (curves a and b), $S_{equ}$ (c), and $S_\infty^\parallel$ (d–g): $\log S_\infty(qR_g)$ vs. $qR_g$ is plotted for $N = 1000$ and different values of $\Theta^*$. (a) $\Theta^* = 5$; $\xi_\parallel/R_g = 62$. (b) $\Theta^* = 1$; $\xi_\parallel/R_g = 24$. (c) $\Theta^* = 0$. (d) $\Theta^* = 0.1$; $\xi_\parallel/R_g = 2.6$. (e) $\Theta^* = 0.2$; $\xi_\parallel/R_g = 5.15$. (f) $\Theta^* = 0.4$; $\xi_\parallel/R_g = 10.2$. (g) $\Theta^* = 0.7$; $\xi_\parallel/R_g = 17.5$. Oscillations appear in the parallel direction when $q_g/q_\xi = \xi_\parallel/2\pi R_g > 1$.

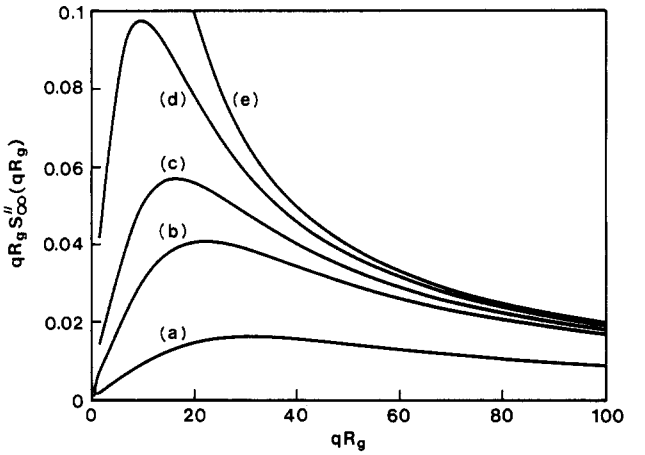


**Figure 5.** Short-wavelength behavior of the steady-state structure factor: $qR_gS_\infty^\parallel(qR_g)$ is plotted as a function of $qR_g$ for $N = 1000$ and different values of $\Theta^*$. (a) $\Theta^* = 5$; $\xi_\parallel/R_g = 62$. (b) $\Theta^* = 1$; $\xi_\parallel/R_g = 24$. (c) $\Theta^* = 0.7$; $\xi_\parallel/R_g = 17.5$. (d) $\Theta^* = 0.4$; $\xi_\parallel/R_g = 10.2$. (e) $\Theta^* = 0$. The linear increase for small $qR_g$ is characteristic of regime VII, (with a slope $\sim n_b/N$) while the $1/qR_g$ decrease at large $qR_g$ is characteristic of regime VIII. The maxima of the curves are at $q \simeq q_b = \xi_\parallel/R_g^2$.

**6.1.3. Diagrams.** Figure 4 shows how the curves $S_\infty^\perp(q)$ vs. $qR_g$ and $S_\infty^\parallel(q)$ vs. $qR_g$ evolve when we increase the electric field. It is clear that very small fields (i.e., $\xi_\parallel \ll R_g$) lead to essentially unmodified spectra. The structure factor decreases (increases) slightly in the parallel (perpendicular) direction, an indication that the chain begins to stretch (shrink); in fact, we see that strong fields ($\theta^* \gg 1$) are needed in order to decrease the transverse dimensions of the chain by a large factor. For intermediate fields ($\xi_\parallel \simeq R_g$), the longitudinal structure factor is seen to decrease rapidly on Figure 4, but since $q_b \simeq q_\xi \simeq q_g$, the regimes studied in section 6.1.2 are not yet present.

At high fields, we have $q_b \gg q_g \gg q_\xi$, and the regimes predicted in the previous subsection are present. The steep decrease of regime V is followed by oscillations (regime VI) having a period $q_\xi$, characteristic of a long-range rodlike structure over a length scale $\simeq 1/q_\xi$. The plateau region

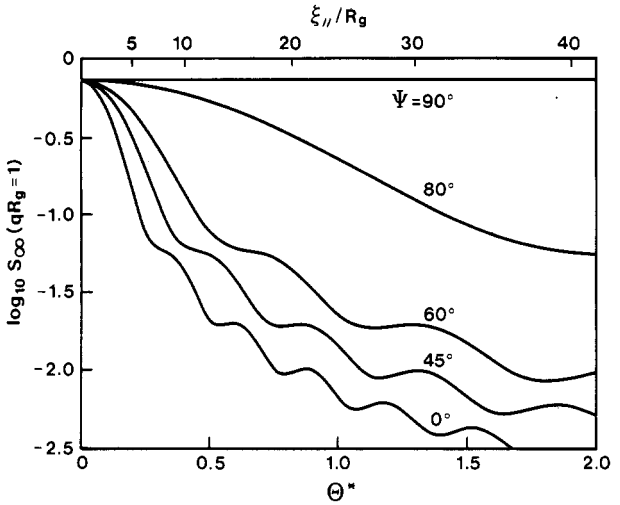


**Figure 6.** Field dependence of the steady-state structure factor: $\log S_\infty(qR_g = 1)$ vs. $\Theta^*(E)$ (lower $x$ axis) and $\xi_\parallel/R_g$ (upper $x$ axis) is plotted for $N = 1000$ and different orientations $\psi$. A sharp decrease happens for $\xi_\psi/R_g \gg 1$. At large $\psi$'s, the chain dimensions are affected only at higher fields (or higher values of $\xi_\parallel/R_g$ and $\Theta^*$) because $\xi_\psi/R_g = (\xi_\parallel/R_g)\cos\psi$.

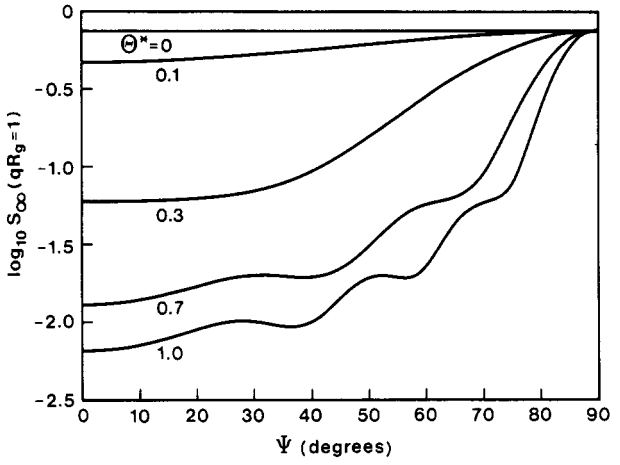


**Figure 7.** Angular anisotropy of the steady-state static structure factor shown on $\log S_\infty(qR_g = 1)$ vs. $\psi$ curves, with $N = 1000$ and different values of $\Theta^*(E)$. Again, large fields are necessary to modify the structure factor near the transverse ($\psi = 90°$) direction.

($q_b > q > q_g$; regime VII) and the short-wavelength regime VIII are more easily identified on Figure 5, where $qR_gS_\infty^\parallel(qR_g)$ is plotted against $qR_g$; the linear part characterizes the plateau regime (the slope giving the field-dependent value of $n_b/N$), and the short-wavelength regime clearly is asymptotic to the $qR_g$ axis.

The high-field limit is found at $\xi_\parallel \gg R_g$ or, from the definitions of both $\xi_\parallel$ and $R_g$, at

$$\frac{q_b}{q_g} = \frac{2\pi q_g}{q_\xi} = \frac{\xi_\parallel}{R_g} = [(6N)^{1/2}\langle\cos\theta\rangle] \gg 1 \qquad (52)$$

This is an interesting result. It means that the longer the chain, the smaller the value of $\langle\cos\theta\rangle$ (or $\theta^* \sim E$) one needs to reach the high-field limit; this is clearly due to the fact that $\xi_\parallel$ ($\sim L$) increases faster than $R_g$ ($\sim L^{1/2}$) as we increase $L$.

The $S_\infty(\mathbf{q})$ vs. $\mathbf{q}$ curves are very much affected by the electric field at $qR_g \simeq 1$ because it is in this wavenumber interval that the derivative of the equilibrium static structure factor $S_{equ}(\mathbf{q})$ is the larger. Figures 6 and 7 suggest following the stretching of the chain by looking at the field and angle dependences of the static structure factor at $qR_g = 1$.

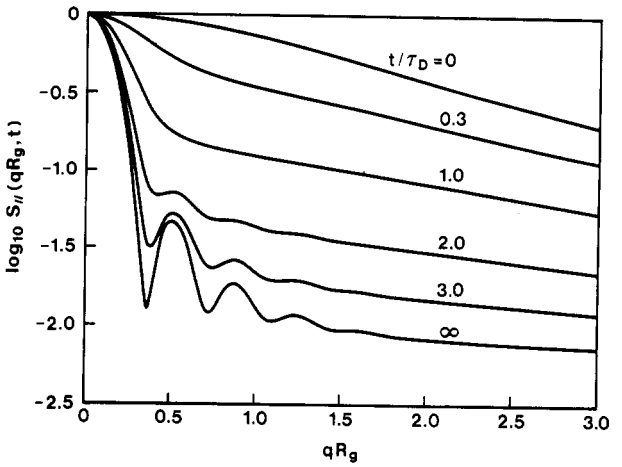


**Figure 8.** Parallel structure factor $S_\parallel(qR_g,t)$ as a function of $qR_g$ for $N = 1000$, $\Theta^* = 0.7$ (or $\xi_\parallel/R_g = 17.5$), and different times $t/\tau_D$. The $t = 0$ condition is given by (34).

On Figure 6, we plotted $\log[S_\infty(qR_g = 1)]$ vs. $\theta^*(E)$ (lower $x$ axis) and $\xi_\parallel/R_g$ (upper $x$ axis) for different values of the angle $\psi$ between $\mathbf{E}$ and the $\mathbf{q}$ vector. The effect of the field is dramatic at $\psi = 0°$: it changes the random-walk conformation by a stretched conformation of size $\sim L\langle\cos\theta\rangle$, leading to a sharp decrease in $S_\infty^\parallel(q)$. Near the transverse direction, the conformation is still a random walk, and we need much higher fields for the chain dimensions to be affected. Finally, we also note that some oscillations are present each time the field is such that a peak would appear at $qR_g = 1$ on a $S_\infty^\psi(q)$ vs. $q$ diagram.

The elongation of the chain in the field direction is accompanied by a slight decrease in its transverse dimensions, and the shape of the chain conformation is an ellipsoid. Figure 7 shows how the static structure factor measures the properties of this ellipsoid. For large fields, one has to go to large angles $\psi$ to see chain dimensions of the order of $R_g$. Curves of $S_\infty(\mathbf{q})$ vs. $\psi$ are therefore good indications of the anisotropy induced by the field. Again, oscillations are present.

**6.2. Time-Dependent Case.** In section 6.1 we studied the exact steady-state structure factor of a chain with charges of opposite signs on its ends, showing that high fields induce stretching and ordering of the chain over a length scale $\xi_\parallel$ in the field direction (in agreement with section 5.1). In section 6.2.1, we show, in agreement with section 5.2, that $\tau_D$ is the relevant time constant when the bias $\delta$ (and hence the longitudinal velocity $v_\parallel$) is negligible. Section 6.2.2 discusses the case $\delta \neq 0$.

**6.2.1. $\delta = 0$ Case.** When $\delta(\mathbf{E}) = 0$, eq 27 reduces to the corresponding equation studied in ref 5, with similar boundary conditions, $a$ being replaced by $X \pm iZ$ (for $p > 0$ and $p < 0$, respectively); from ref 5, we then obtain

$$S(\mathbf{q},t) = \mathrm{Re}\left\{D(X - iZ) + (1/6)(X - iZ - \beta) \times (1 + e^{-(X-iZ)})H[X - iZ,t] + (1/6)(X - iZ - \beta)^2 e^{-\beta}\int_0^1 dy\, y^3 e^{\beta y}(1 + e^{-(X-iZ)y})H[(X - iZ)y, t/y^2]\right\} \qquad (53)$$

where it is assumed that the initial condition is given by $F_0(s,p,\mathbf{q},t = 0) = e^{-\beta p}$. The $H$ function is defined by

$$H(x,t) = \frac{96}{\pi^2}\sum_{n\ \mathrm{odd}} \frac{1}{n^2(n^2\pi^2 + x^2)} e^{-n^2 t/\tau_D} \qquad (54)$$

When the initial condition is one of equilibrium, i.e., $\beta = x^{(0)}$, (53) indicates how chains evolve from random-walk to stretched conformations (Figures 8–10) over the time scale $\tau_D$.

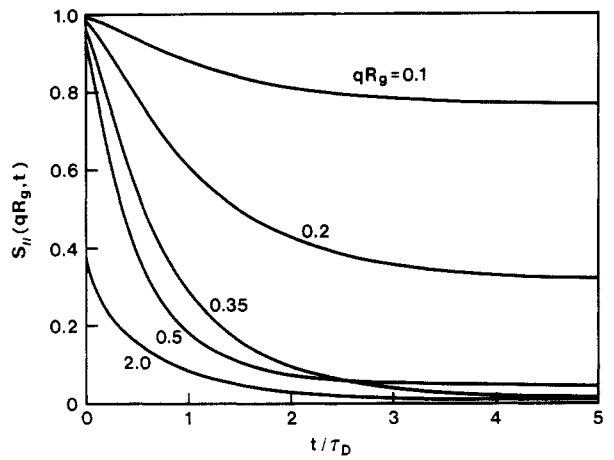


**Figure 9.** Parallel structure factor $S_{\parallel}(qR_g,t)$ as a function of time for $N = 1000$, $\Theta^* = 0.7$ (or $\xi_{\parallel}/R_g = 17.5$), and different values of $qR_g$. The $t = 0$ condition is given by (34).

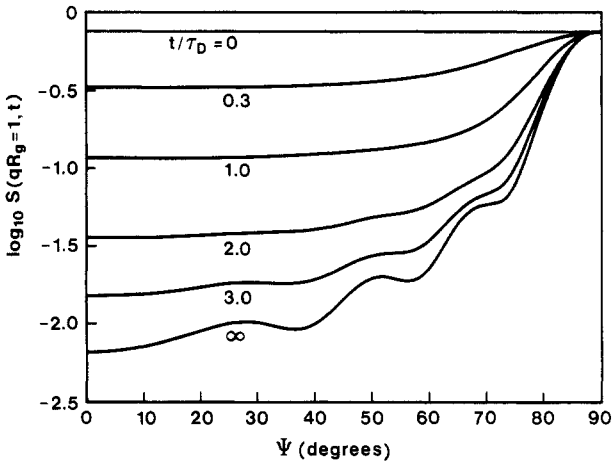


**Figure 10.** Time evolution of the angular anisotropy of the structure factor: $\log S(qR_g = 1,t)$ is plotted as a function of $\psi$, with $N = 1000$, $\Theta^* = 1$ (or $\xi_{\parallel}/R_g = 24$), and different values of $t/\tau_D$. The $t = 0$ condition is given by (34).

Figure 8 shows the time dependence of the (parallel) static structure factor when, at $t = 0$, we apply a field such that $q_b \gg q_g \gg q_\xi$. It illustrates how the random jumps in the tube bring in new conformations when the averages $\langle\cos\theta\rangle$ and $\langle\cos^2\theta\rangle$ are modified by the field. Most of the stretching occurs between $t = 0$ and $t = \tau_D$, and accordingly it is during this period that $S_{\parallel}(q,t)$ decreases substantially. For longer times, all the chains have undergone tube renewal, and the peaks between $q = q_\xi$ and $q = q_g$, characteristic of a new rodlike conformation with longitudinal length scale $\approx 1/q_\xi$, appear.

The fact that $\tau_D$ is indeed the relevant relaxation time is exemplified even more clearly in Figure 9, where the time evolution of $S_{\parallel}(q,t)$ is shown for some chosen values of $qR_g$. Note that the curves for $qR_g = 0.35$ and $qR_g = 0.5$ cross each other, a situation arising from the peaks present at low wavenumbers on Figure 8.

Finally, Figure 10 illustrates the time dependence of the different dimensions of the chain. The final anisotropic conformation is reached after $t \approx 3\tau_D$.

Very large or very small values of $\theta^*$, as well as $S_{\perp}(q)$, are of no special interest; in all cases, $\tau_D$ remains the characteristic time involved, as discussed in section 5.2. Figures 8–10 show the more interesting time-dependent phenomena.

**6.2.2. General ($\delta \neq 0$) Time-Dependent Case.** When $\delta(\mathbf{E}) \neq 0$, one has to find $A_+(p)$ and $A_-(p)$ in (28) from the boundary conditions (22). However, it has not been possible to obtain this general solution analytically for conditions (41).

From the discussion of section 5.2, it is clear that a numerical analysis of the general time-dependent case would give results similar to the ones presented in section 6.2.1, except that the time scale of the stretching would be $\tau_D$ for small fields and $\tau_E$ (as defined by (38)) for large fields. The solution would give additional details on the relaxation of the initial (random-walk) conformation toward the steady-state (stretched) conformation. Equation 40 gives the field-dependent bias necessary to reach the crossover between the two regimes ($\tau_D$- and $\tau_E$-driven stretching) for a time-independent bias.

**6.3. Conclusions.** The case studied in this section is the simplest nontrivial one from the theoretical point of view: $\delta$ cannot change its sign in time, and the equations presented in section 3 give exact results in many situations. However, the time-dependent $\delta \neq 0$ solutions have not been found analytically.

Experimentally, it represents an interesting challenge. Although such molecules can be synthesized in principle, the experimental parameters one would have to work with are not obvious. In particular, the problem of charge–charge interactions may prove difficult to solve.

This calculation shows how the mathematical apparatus developed here can be used to study the stretching of charged polymers in electric fields; the results agree with eq 42 and 43 in the steady state and with section 5.2 for the time-dependent case.

With the technique developed by Boué et al.[6] it should be possible to measure $S(\mathbf{q},t)$ vs. $q$, $t$, $E$, or $\psi$ by small-angle neutron scattering (SANS). The time and length scales should be identifiable, and the microscopic parameters of the system can be obtained through the measurement of the $\tau$'s and $\xi_\psi$'s. Evidence of the overall anisotropy of the chain conformations is also of interest. Figures 4–10 suggest experimental avenues to explore.

It is of interest here to compare the result of this section to the static properties of a chain under traction[14] and of a chain trapped into a tube.[15]

Benoit et al.[14] studied the problem of a deformed polymer coil and found results that are similar to ours in some limits. In fact, their parameters $b$ ($\sim\langle\cos\theta\rangle$ in our notation) and $\lambda_{\parallel}$ ($\sim\langle\cos^2\theta\rangle$) are independent, which is not the case here. However, they did not investigate the regime where oscillations appear. Recently, Kremer and Binder[15] presented a scaling theory and Monte Carlo simulation results for polymer chains confined into tubes. Their results for the static properties of the chains are very similar to ours. In their case, the tube radius acts as an effective blob radius $b$. Both the scaling analysis and the simulation predict a plateau regime and some oscillations in the structure factor for $b < R_g$, i.e., when the tube reduces the lateral dimensions of the chain. In both studies, however, the similarities with our work are restricted to the time-independent properties as the mechanisms by which the chains change their conformations are fundamentally different; in our case, the relaxation of chain conformations by reptation can even be tuned by the field through the value of the bias $\delta(\mathbf{E})$.

## 7. Example 2: Uncharged End Segments

We assume here that the segments $\mathbf{r}_1$ and $\mathbf{r}_N$ are uncharged, and we make no assumption about the charge of the other segments $\mathbf{r}_i$ ($1 < i < N$). With $Q_1 = Q_N = 0$ (see Figure 2d), we have $\langle\cos\theta\rangle = 0$ and $\langle\cos^2\theta\rangle = {}^1/_3$ for both ends and, consequently, $z_{1,N} = 0$ and $x_{1,N} = x^{(0)} = q^2R_g^2$. However, the bias $\delta(\mathbf{E})$ is not necessarily zero; depending

on the details of the charge distribution, it may even be time-dependent.

This case is simply a subset of the more general one presented in section 6. The steady-state (47) reduces to

$$F_\infty(s,p,\mathbf{q}) = e^{-x^{(0)}p} = e^{-q^2R_g^2p} = F_{equ}(s,p,\mathbf{q}) \quad (55)$$

from which we conclude that no stretching can take place with an initial condition $F_0 = F_{equ} = e^{-x^{(0)}p}$, since the ends cannot align in any special direction.

However, if the initial condition is given by $F_0 = e^{-\beta p}$, with $\beta \neq x^{(0)}$, the relaxation toward the equilibrium state $F_{equ} = e^{-x^{(0)}p}$ is characterized by the general solution (28)–(30). Although no analytic solution has been found for $A_+$ and $A_-$, the discussion in sections 5.2 and 6.2.2 also applies here: for $\delta \to 0$ the relaxation toward state $F_{equ}$ takes a time $\tau_D$, as in ref 5, while for $\delta > \pi^2/2N$, the relaxation is very much accelerated by the electric drift and takes place in a time $\tau_E < \tau_D$. *In either case*, $R_g$ remains the relevant steady-state length scale.

This simple case is extremely important. In fact, it is easy to synthesize a molecule such as the one described in Figure 2d. A study of this case should easily distinguish between the important time scales since the crossover between the $\tau_D$ and $\tau_E$ regimes is accessible. From a measure of $\tau_E(\mathbf{E},L)$, for instance, parameters such as $\langle v_l \rangle$, $a$, the total charge $\sum Q_i$, and/or $L$ can be obtained.

## 8. Discussion

The BRM has three main ingredients. First, it assumes that the tube concept of the zero-field reptation theory[1-3] is still valid in the presence of an electric field, i.e., that the entanglements of the chains can be replaced by a fixed open-ended tube in which the chain is forced to move. Second, it assumes that the electric field aligns the charged end segments ($\mathbf{r}_1$ and/or $\mathbf{r}_N$) in a time $<\Delta t$: a Boltzmann factor can then be defined to calculate the probabilities of the possible orientations of these segments. Lastly, it transforms the random Brownian motion along the tube into a biased motion to take into consideration the field-induced longitudinal drift.

Computer simulation is the most straightforward technique to study the dynamics of charged chains in the BRM, and particularly their static structure factor. A general charge distribution can then be used, the exact instantaneous bias $\delta(\mathbf{E},t)$ can be calculated for each chain, and even the charge–charge interactions can be taken into account while calculating the instantaneous values of $\delta(\mathbf{E},t)$ and $\theta^*$.

In this paper, we have developed the general framework for such simulations. According to which effects one wants to take into consideration, $\theta^*$ (see (6)) may or may not include the internal electric field induced by the charges themselves. More important, however, would be to consider the exact conformation-, field- and time-dependent bias $\delta(\mathbf{E},t)$ which, again, may or may not include internal field effects.

A universal (i.e., $\delta(\mathbf{E},t)$-independent) criterion for the field-induced stretching of the chains is that the anisotropic conformation length $\xi_\psi \equiv L|\cos\psi|\langle\cos\theta\rangle$ has to be larger than $R_g$, the isotropic length scale characterizing the equilibrium state. For the directions $\psi$ where $\xi_\psi < R_g$, the steady state is essentially unmodified, while stretching is expected for $\xi_\psi > R_g$. These results were obtained from the boundary conditions of the structure factor in the BRM, which are always valid in a constant electric field, and are in agreement with the specific analytic solution presented in section 6.

The identification of a time constant $\tau_E$ for the electric field induced tube disengagement follows naturally from the assumption of a constant $\delta(\mathbf{E})$ and the associated nonzero conformation-independent longitudinal velocity $v_l$. However, it must be stressed that in general $F_l$, and hence $\delta$, is a complicated function of the charge distribution along the chain and of the instantaneous chain conformation; in this case, the relation between $\tau_E$ and $\delta(\mathbf{E})$ is not straightforward (see (37)).

We classified charged chains into four groups (Figure 2). Class a is interesting because it leads to exact results (section 6) when $\delta(\mathbf{E})$ is constant (or when an appropriate average bias $\langle\delta(\mathbf{E})\rangle$ can be defined in (20)). It is equivalent to pulling the ends of the chain apart by a tunable force proportional to $Q_{1,N}\mathbf{E}$. Class b contains uniformly charged polymers such as polyelectrolytes. A SANS experiment would be important here as it would lead to a better understanding of the behavior of DNA in gel electrophoresis. Theories concerning DNA stretching exist,[7-11] but detailed verification of the processes involved is still needed. Class c polymers are expected to be easy to synthesize and are of some technological importance. Finally, class d charged polymers show accelerated disengagement of the chains from their tube without accompanying tube deformation (section 7); this could give information on the importance of the end segments in the theory of reptation.

For all four classes, the radius of gyration $G_\perp$ is expected to be proportional to $R_g$ and to vary very slowly with the electric field. The longitudinal radius of gyration $G_\parallel$ is also proportional to $R_g$ at small fields but increases slowly instead of decreasing, indicating an increase of the path length of the random walk in this direction. At high fields, stretching occurs as $G_\parallel \sim \xi_\parallel \sim L$. These behaviors have been shown clearly for a special case in section 6. Measurement of $S_\infty(\mathbf{q})$ vs. $\mathbf{q}$ would give information about $R_g$, $\xi_\perp$, and $\xi_\parallel$ and therefore about the parameters $L$, $a$, and $\theta^*$. These results are expected to correlate with the theory presented in section 6 and to be interpretable in a similar way for any class of charged chains or any charge distribution. Information concerning $\xi_\psi$ should thus be a good way to characterize charged chains and their environment.

As shown (at least approximately) by (40), "high" levels of $\delta$-biasing should be easily obtainable in actual cases for long chains ($N$ large). For example, assume a polymer with a charge $Q_N$ only on its $\mathbf{r}_N$ segment (class c; Figure 2c); other cases, with more charges, would give higher biases. As the $\mathbf{r}_N$ segment changes its orientation in the electric field very quickly (each $\Delta t$), the average longitudinal force is given by

$$\langle F_l \rangle = QE\langle\cos\theta\rangle \quad (56)$$

from which (using (11) and (7c))

$$\delta = \frac{QEa\langle\cos\theta\rangle}{2k_BT} \simeq \left(\frac{QEa}{12^{1/2}k_BT}\right)^2 \simeq 10^{-8}\left[\frac{Q[\mathrm{e}]E[\mathrm{V/cm}]a[10^3\ \text{Å}]}{T[300\ \mathrm{K}]}\right]^2 \quad (57)$$

where, in the last part, $Q$ is in units of the electron charge e, $E$ is in V/cm, $a$ is measured in units of 1000 Å, and $T$ is 300 K. For $E \simeq 30$ V/cm and $Q \simeq 100e$, this gives $\delta \simeq 0.1$, which is quite large compared to $\pi^2/2N$ (see (40)) for long chains ($N > 50$). The whole interval of interest for $\delta$ is therefore expected to be readily accessible in experiments involving long chains.

Charged polymers are not easily studied in the reptation regime. Dense solutions of charged polymers cannot be used since charge–charge interactions would then be overwhelming. Very dilute solutions of charged polymers in

a neutral polymer matrix are necessary in order to have noninteracting charged molecules. Another experimental avenue is to use gels. As for DNA gel electrophoresis, the gel would provide a neutral and stable source of chain entanglements for the reptating chain. The average pore size can be identified with the parameter $a$, which can be changed for different gels.

Measurement of relaxation times using SANS can be carried out by using the technique developed by Boué et al.[6] This experiment could give the time scale involved in chain stretching and, in particular, the time scale related to the pulsed field experiments, of interest at the present time.[7-9] More generally, $\tau_D$ and $\tau_E$ would give information about factors such as $\langle\delta\rangle$ (or $\langle v_\parallel\rangle$), $a$, $L$, and $D_c$.

Computer simulation would clearly provide us with more information concerning both the steady-state and transient properties of stretched charged polymers in electric fields. Comparison with experiments would be a good test for the BRM in particular, and the concept of reptation in general. Because the electric field is a tunable parameter which can be used to change both the time and length scales involved, new measurements of the physical parameters and better characterization of the system under study are expected.

**Acknowledgment.** G.W.S. acknowledges receipt of an Industrial Postdoctoral Fellowship from the Natural Sciences and Engineering Research Council of Canada.

## Appendix A. Radius of Gyration for Class a Chains

The average radius of gyration $G^2$ is defined as[16]

$$G^2 = \langle \sum_{i=1}^{N} S_i^2/N \rangle \tag{A1}$$

where $S_i$ is the distance between the $i$th segment and the center-of-mass of the chain. The sum is over the $N$ segments $\mathbf{r}_i$ (see section 2), and the $\langle ... \rangle$ average is over all chain conformations. The theorem of Lagrange[16] allows us to write

$$G^2 = (1/N^2)\langle \sum_{1\le i<j\le N} r_{ij}^2 \rangle \tag{A2}$$

where $r_{ij}$ is the distance between the $i$th and the $j$th segments.

In order to compute $G^2$ from (A2), we first calculate some moments of the end-to-end distance $\mathbf{h}$. By definition, the end-to-end distance of a chain of $N$ vector segments $\mathbf{r}_i$ is given by

$$\mathbf{h} = \sum_{i=1}^{N} \mathbf{r}_i \tag{A3}$$

With a bias $\delta$, a fraction $f(\delta)$ of the $N$ segments (on the average) have been oriented by the (say) $\mathbf{r}_1$ end segment, while the other $N(1 - f(\delta))$ segments have been oriented by the $\mathbf{r}_N$ end segment. The actual value of the fraction $f(\delta)$ is not important in this discussion but can be calculated easily.[17] Assuming that the average properties of each end segment determine the average properties of all the segments they have oriented (the tube assumption), we separate the summation in (A3) in two parts to obtain

$$\langle \mathbf{h} \rangle = \langle [\sum_{i=1}^{f(\delta)N} \mathbf{r}_i] + [\sum_{i=f(\delta)N+1}^{N} \mathbf{r}_i] \rangle = f(\delta)N\langle \mathbf{r}_1 \rangle + N[1 - f(\delta)]\langle \mathbf{r}_N \rangle \tag{A4}$$

This equation is general and applies for all four classes of charged chains (see section 5 and Figure 2) if the bias $\delta$ is a conformation-independent constant. For $Q_1 = -Q_N = Q$ (class a chains) we have $\langle \mathbf{r}_1 \rangle \cdot \hat{x} = \langle \mathbf{r}_N \rangle \cdot \hat{x} = a\langle \cos\theta \rangle_Q$, with $\langle \cos\theta \rangle_Q$ given by (7) and (A4) then leads to

$$\langle h_x \rangle = Na\langle \cos\theta \rangle_Q = \xi_\parallel \tag{A5}$$

as expected. Interestingly enough, this case shows a $\delta$-independent $\langle h_x \rangle$. This result means that since both ends stretch the chain the same way, the $\delta$-bias is irrelevant. For all other cases, including class a chains with $Q_1 \neq -Q_N$, the moments of $h$ would depend on $\delta$ as well, rendering the problem more difficult.

Similarly, one can calculate other moments of $\mathbf{h}$ in any direction $x,y,z$. Of particular interest here are the following results for $Q_1 = -Q_N = Q$:

$$\langle h_{y,z}^2 \rangle = \tfrac{1}{2}Na^2\langle \sin^2\theta \rangle_Q \tag{A6}$$

$$\langle h_x^2 \rangle = Na^2\langle \cos^2\theta \rangle_Q + N(N-1)a^2\langle \cos\theta \rangle_Q^2 \tag{A7}$$

Again, the bias $\delta$ is irrelevant for this case.

Using (A6) to evaluate $r_{ij}$ in eq A2 (this can be done because the previous result does not depend on the bias $\delta$), we obtain (for $N \gg 1$)

$$G_{y,z}^2 = (1/N^2) \sum_{1\le i<j\le N} \frac{j-i}{2} a^2\langle \sin^2\theta \rangle_Q \simeq \frac{Na^2}{12}\langle \sin^2\theta \rangle_Q \tag{A8}$$

which reduces to $G_{y,z}^2 = {}^1/_3 R_g^2$ for $E = 0$ since, from (8a), $\langle \sin^2\theta \rangle_0 = 1 - \langle \cos^2\theta \rangle_0 = {}^2/_3$. Using (A7) and (A2), we also obtain ($N \gg 1$)

$$G_x^2 = (1/N^2) \sum_{1\le i<j\le N} [(j-i)a^2\langle \cos^2\theta \rangle_Q + (j-i) \times (j-i-1)a^2\langle \cos\theta \rangle_Q^2] \simeq \frac{Na^2}{6}\langle \cos^2\theta \rangle_Q + \frac{N^2a^2}{12}\langle \cos\theta \rangle_Q^2 \tag{A9}$$

which reduces to $G_x^2 = {}^1/_3 R_g^2$ for $E = 0$.

The following limits of (A8) and (A9) are of interest:

$$\lim_{E\to 0} [G_x^2 + G_y^2 + G_z^2] = R_g^2 \tag{A10}$$

$$\lim_{E\to \infty} [G_x^2 + G_y^2 + G_z^2] = L^2/12 \tag{A11}$$

The first result is typical of a random-walk conformation, while the second (for which $G_{y,z}^2 = 0$) is characteristic of a rod of length $L$ parallel to $\hat{x}$.

## References and Notes

(1) de Gennes, P.-G. *J. Chem. Phys.* **1971**, *55*, 572.
(2) Edwards, S. F. *Proc. Phys. Soc. London* **1967**, *92*, 9.
(3) Doi, M.; Edwards, S. F. *J. Chem. Soc., Faraday Trans. 2* **1978**, *74*, 1789.
(4) Hong, K. M.; Noolandi, J. *Makromol. Chem., Rapid Commun.* **1983**, *4*, 617.
(5) Noolandi, J.; Hong, K. M. *J. Phys., Lett.* **1984**, *45*, L-149.
(6) Boué, F.; Nierlich, M.; Jannink, G.; Ball, R. C. *J. Phys., Lett.* **1982**, *43*, L-585.
(7) Slater, G. W.; Noolandi, J. *Phys. Rev. Lett.* **1985**, *55*, 1579.
(8) Slater, G. W.; Noolandi, J. *Biopolymers* **1985**, *24*, 2181.
(9) Slater, G. W.; Noolandi, J. *Biopolymers* **1986**, *25*, 431.
(10) Lumpkin, O. J.; Déjardin, P.; Zimm, B. H. *Biopolymers* **1985**, *24*, 1573.
(11) Lumpkin, O. J.; Zimm, B. H. *Biopolymers* **1982**, *21*, 2315.
(12) For a given chain at a given time $t$, the value of $\theta^*_{1,N}(\mathbf{E})$ and $\delta(\mathbf{E},t)$ could, in principle, take into account the charge–charge interactions in the system. However, these effects depend on factors such as the charged chain concentration, counterions, dielectric constant, charge distribution on each chain, etc., and would make the problem intractable. In our use of the BRM, we consider a single (effective) chain in an uncharged environment and in the presence of an electric field, neglecting the interactions between the charges of the same chain. As long as the chain moves in a tube, other effects are not expected to modify the qualitative picture given in section 5.
(13) Slater, G. W.; Noolandi, J. *Europhys. Lett.* **1986**, *1*, 347.
(14) Benoit, H.; Duplessix, R.; Ober, R.; Daoud, M.; Cotton, J. P.; Farnoux, B.; Jannink, G. *Macromolecules* **1975**, *8*, 451.
(15) Kremer, K.; Binder, K. *J. Chem. Phys.* **1984**, *81*, 6381.
(16) Flory, P. J. "Statistical Mechanics of Chain Molecules"; Interscience: New York, 1969; Appendix A.
(17) Slater, G. W.; Noolandi, J. to be submitted for publication.